

Perching and Grasping Using a Passive Dynamic Bioinspired Gripper

Amir Firouzeh^{ID}, Jongeun Lee^{ID}, Hyunsoo Yang^{ID}, Member, IEEE, Dongjun Lee^{ID}, Member, IEEE,
and Kyu-Jin Cho^{ID}, Member, IEEE

Abstract—The ability to grasp objects broadens the application range of unmanned aerial vehicles (UAVs) by allowing interactions with the environment. The difficulty in performing a midair grasp is the high probability of impact between the UAV’s foot and the target. For a successful grasp, the foot must smoothly absorb the energy of impact and simultaneously engage with the target in a short period of time. We present a bioinspired passive dynamic foot in which the claws are actuated solely by the impact energy. Our gripper simultaneously resolves the issue of smooth absorption of the impact energy and fast closure of the claws by linking the motion of an ankle linkage and the claws through soft tendons. We study the dynamics of impact and use the stiffness of the tendon as our design/control parameter to adjust the mechanics of the gripper for smooth recycling of the impact energy. Our gripper closes within 45 ms after initial contact with the impacting object without requiring any controller or actuation energy. An electroadhesive locking mechanism attached to the tendon locks the claws within 20 ms after reaching closed configuration. We demonstrated the effectiveness of our gripper by integrating it in an UAV and performing a variety of passive dynamic perching and grasping tasks.

Index Terms—Aerial systems: mechanics and control, compliant mechanism, passive dynamic gripper, underactuated robots.

I. INTRODUCTION

THE reliability of birds’ perching can be partially attributed to the morphology of their feet and legs that allows recycling of the impact energy for closing the claws within a few hundredths of a second [1], [2]. A mechanical feedback loop in avian feet couples the folding motion of the ankle joint and the flexion of the claws. This coupling, which is referred to as automatic digital flexor mechanism (ADFM) [3], [4], [5],

happens due to the routing of the digital tendons around the ankle joint; see Fig. 1(a). After the closure of the claws, a ratchet-like structure inside the tendon sheath [6], [7], [8] automatically locks the tendons and claws. Together, these elements build a mechanism that is referred to as automatic perching mechanism. Replicating such a mechanism in a robotic gripper would allow robust and reliable dynamic grasp in the presence of impact, which is specifically desirable for application in unmanned aerial vehicles (UAVs).

Inspired by the embodied intelligence of birds’ feet, passive perching devices were developed that engage under the weight of the UAV in quasi-static condition [9], [10], [11], [12], [13]. Bioinspired grippers capable of dynamic perching have also been developed [14], [15], [16], [17], [18], [19], [20], [21]. The automatic closure of these gripper allows successful perching with minimal control effort. The closure of the claws in the majority of these bioinspired dynamic grippers, however, relies on additional energy from a spring element [14], [15], [16], [17], [18]. In these devices, the recycling of the impact energy is not essential, and therefore, is not fully investigated. Empirical data on perching using fully passive dynamic grippers [20] have shown the possibility of perching by solely relying on the impact energy. However, establishing a design framework for a gripper that can effectively recycle the impact energy, based on the mass and velocity of the impacting objects, requires further analysis. In specific, studying the importance of the stiffness of the digital tendon in avian automatic perching mechanism and its robotic counterparts is necessary, and is currently missing. The results of such a study will be applicable in designing both passive and active grippers that are resilient to (and can even benefit from) impact.

In this article, we present the concept of soft coupling in a bioinspired passive dynamic gripper. Our gripper uses a nimble Sarrus linkage, which is realized based on smart composite microstructures (SCM) framework [22], [23], [24], as its ankle linkage. A soft tendon links the motion of this linkage to the rotation of the claws; see Fig. 1(b). By studying the dynamics of impact, we develop a design framework for the tendon stiffness, based on the mass and velocity of the impacting objects, for smooth absorption and transfer of the impact energy.

To lock the claws in closed configuration, we developed a tendon locking mechanism based on electroadhesive clutches [25], [26]. This locking mechanism engages within 20 ms after activation and locks the configuration of the claws. The locking mechanism weighs 10 g and can withstand up to 100 N of tension

Manuscript received 16 April 2023; revised 25 August 2023; accepted 4 November 2023. Date of publication 24 November 2023; date of current version 15 December 2023. This paper was recommended for publication by Associate Editor S. Briot and Editor M. Yim upon evaluation of the reviewers’ comments. This work was supported by the National Research Foundation of Korea (NRF) Grant funded by the Korean Government (MSIT) under Grant RS-2023-00208052. (Corresponding author: Kyu-Jin Cho.)

Amir Firouzeh, Jongeun Lee, and Kyu-Jin Cho are with the Biorobotics Laboratory, Department of Mechanical Engineering, SNU-IAMD, Institute of Engineering, Seoul National University, Seoul 08826, South Korea, and also with the Soft Robotics Research Center, Seoul National University, Seoul 08826, South Korea (e-mail: amir.firouzeh@epfl.ch; yhjelee@snu.ac.kr; kjcho@snu.ac.kr).

Hyunsoo Yang and Dongjun Lee are with the Interactive and Networked Robotics Laboratory, Department of Mechanical Engineering, SNU-IAMD, Institute of Engineering Research, Seoul National University, Seoul 08826, South Korea, and also with the Soft Robotics Research Center, Seoul National University, Seoul 08826, South Korea (e-mail: yangssoo@snu.ac.kr; djlee@snu.ac.kr).

This article has supplementary downloadable material available at <https://doi.org/10.1109/TRO.2023.3336216>, provided by the authors.

Digital Object Identifier 10.1109/TRO.2023.3336216

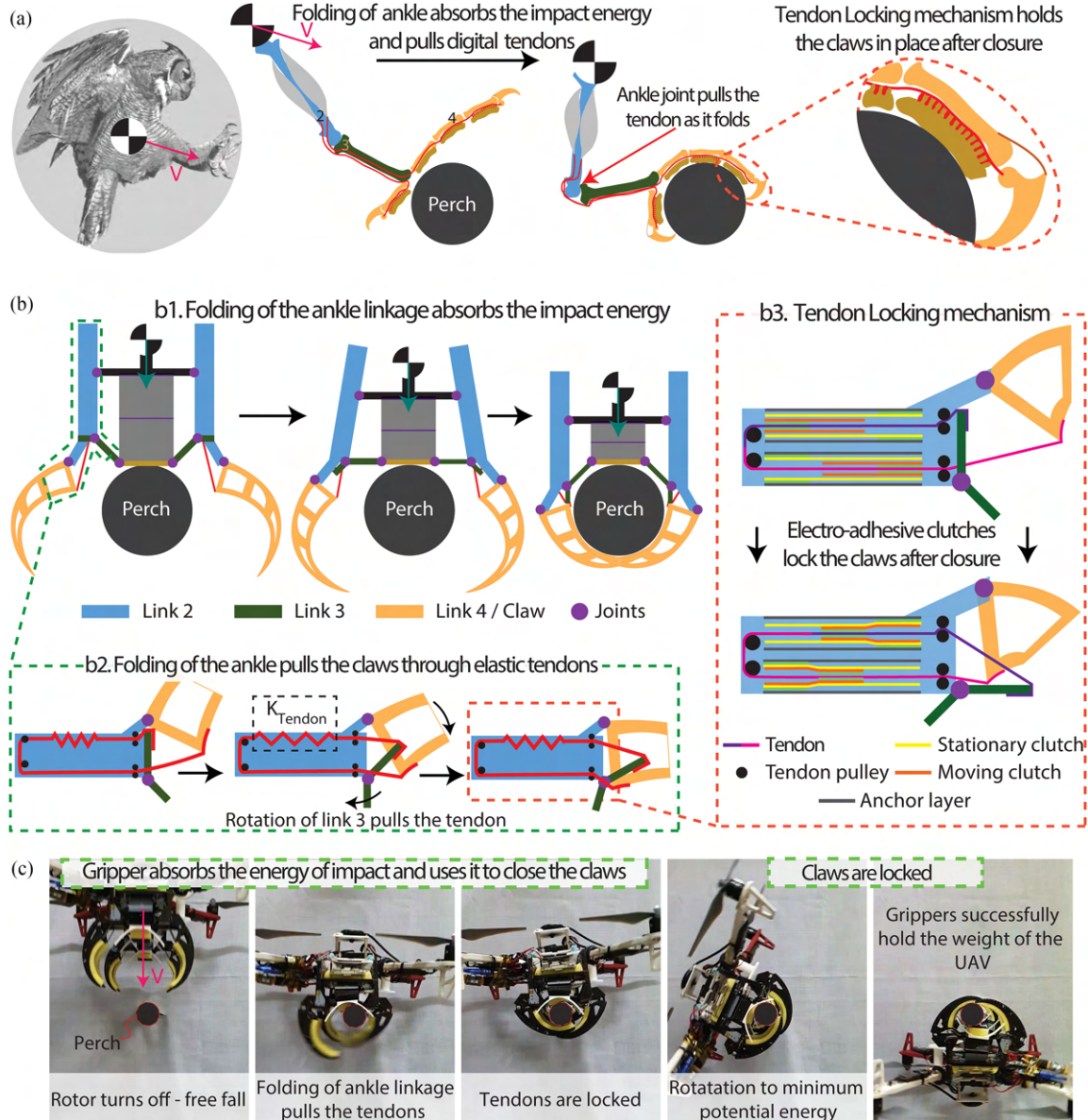


Fig. 1. Passive dynamic grasp through recycling impact energy. (a) In avian automatic perching mechanism, the folding of the ankle joint pulls the digital tendons and automatically closes the claws. Then, a tendon locking mechanism holds the claws in closed configuration. (b) In our passive dynamic gripper, (b1) Sarrus linkage has the role of the ankle joint and pulls the tendon as it folds; (b2) soft tendon links the motion of ankle and claws; and (b3) electroadhesive clutches that are integrated on the tendon have the role of the tendon locking mechanism. (c) We used two grippers as the feet of an UAV for performing passive dynamic perching and grasping; videos of the drone experiments are in the supplementary information.

in the tendon, which translates into a 4-kg loading capacity for a gripper that weighs 150 g. We also used the electroadhesive clutches in a version of the gripper with variable stiffness tendons to demonstrate the feasibility of using the tendon stiffness as a control parameter to adjust the mechanics of the gripper according to the impact conditions.

To demonstrate the performance of our passive dynamic gripper, we integrated two grippers (the version with fixed tendon stiffness) as the feet of a 1.8-kg UAV [see Fig. 1(c)], and performed perching maneuver on a 35-mm diameter cylindrical bar at different inclinations ($0\text{--}20^\circ$) and on a 20-mm diameter rope. We also verified the possibility of performing pick and place

tasks by transferring a series of objects with diameters ranging from 20 to 50 mm, including a fragile light tube, for the videos of the drone experiments refer to the supplementary information.

II. DESIGN AND MANUFACTURING

The avian automatic perching mechanism consists of the following three key components:

- 1) an ankle that folds and provides the necessary range of motion for smooth energy absorption during impact;
- 2) digital tendons that transfer the absorbed energy to the claws;

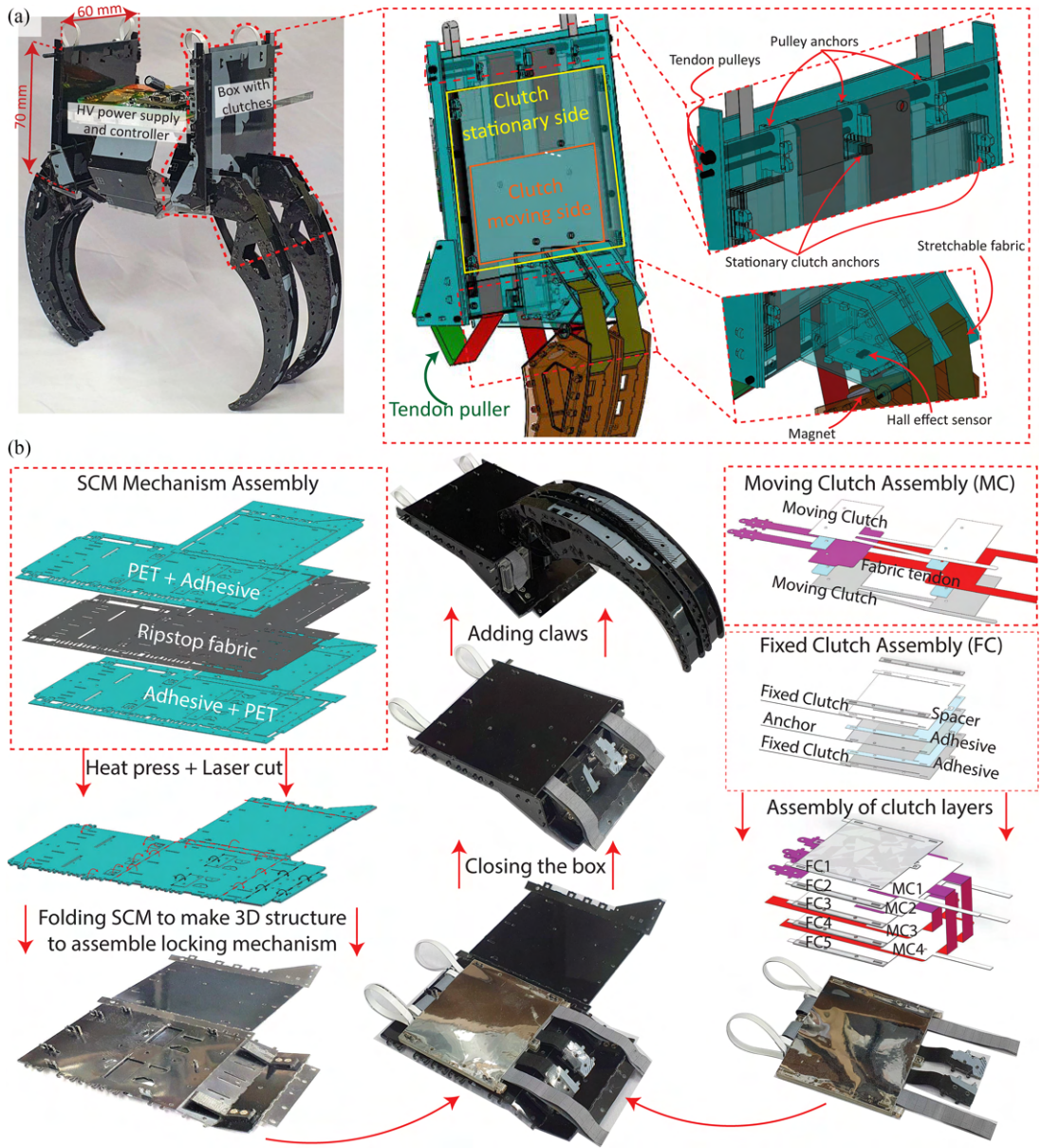


Fig. 2. (a) Passive dynamic gripper including its high-voltage power supply and control/communication board. The electroadhesive clutches are housed inside the ankle linkage. A series of pulleys route the tendon (which connects the tendon puller to the claws) inside the ankle linkage. A Hall effect sensor inside the claw measures its angle. (b) Components of gripper (electroadhesive tendon locking mechanism and the SCM structure) are fabricated by stacking laser cut layers and bonding them inside a jig in a heated press. The SCM sheet is folded to make the 3-D scaffolding for assembling the tendon locking mechanism. The routing of the tendon is designed to be contained in one side of the Sarrus linkage for easy assembly. The claws are manufactured separately and assembled onto the scaffolding.

- 3) ratchet-like features in the tendon sheath that lock the tendons at close proximity to the distal joints to hold the claws closed; see Fig. 1(a).

Our gripper [see Fig. 1(b)] consists of the following similar three components:

- 1) a Sarrus linkage at the base of the gripper plays the role of the ankle joint and folds under impact [see Fig. 1(b1)];
- 2) an elastic tendon links the motion of the Sarrus linkage to the claws [see Fig. 1(b2)];
- 3) a tendon locking mechanism, based on electroadhesive clutches, locks the position of the claws in the closed configuration [see Fig. 1(b3)].

The elastic tendon makes a soft coupling between the ankle mechanism and the claws. Elongation of the tendon is desired in the energy absorption phase of a passive dynamic grasp for smooth energy transfer. In the holding phase, however, tendon elongation will result in claw recoil and opening of the gripper. To prevent this, a key design objective was the proximity of the locking mechanism and the claws. In the avian feet and our gripper, the locking mechanism is placed at the distal portion of the digital tendons right before connection to the claws. To fulfil this design objective, we developed a compact locking mechanism based on electroadhesive clutches; see Fig. 2. High loading capacity per unit mass (10 N/g), fast activation (within 20 ms),

and possibility of integration on tendons make electroadhesive clutches a desirable choice for the locking mechanism in our passive dynamic gripper.

The electroadhesive clutch layers are fabricated following the recipe by Diller et al. [25], [26] using a 50-μm aluminized PET sheet as substrate and Luxprint 8153/Dupont as the dielectric layer, with a combined thickness of 85–90 μm. The high permittivity of the dielectric layer allows activation of the clutches at relatively low voltages, 350 V. The nontacky surface of the dielectric layers helps with the smooth sliding of the layers when the voltage is removed. Fig. 2(b) presents the integration process of the electroadhesive clutching pairs on the tendons and integration of the overall locking mechanism into the ankle linkage. The mass of the electroadhesive tendon locking mechanism, including the fixed layers, is under 10 g, which guarantees a negligible effect on the dynamic behavior of the gripper. The eight clutch pairs in this assembly provide around 100 cm² of clutching area that produces 100 N of tendon locking force at 350 V.

We integrated a custom-made high-voltage power supply and controller board in the base of the gripper; see Fig. 2(a). This board makes the grippers compact and self-sufficient for easy application as an UAV foot. A CurieNano/DFRobot board controls the voltage setting of the high-voltage power supply and based on the Bluetooth command initiates the perching sequence. The controller activates electroadhesive clutches when the claws are closed.

The ankle linkage is realized based on the SCM design and manufacturing frameworks [22], [23], [24], Fig. 2(b). SCMs are quasi-2D composite sheets of two stiff layers (in our case a 0.35-mm adhesive backed PET sheet) sandwiching a flexible hinge layer (in our case Ripstop fabric). A cutting pattern in the stiff layer exposes desired sections of the hinge layer to produce flexure joints that define the degrees of freedom and kinematics of the mechanism. The large loading capacity per unit mass of SCM mechanisms makes them nimble [27], [28], [29] and a good choice for our highly dynamic application. Moreover, its quasi-2D nature provides the large surface areas that is required to house electro-adhesive tendon locking mechanism.

The 3-D scaffolding for anchoring the fixed clutch layers and holding the pulleys, which route the tendons inside the ankle joint, are realized by folding the SCM structure as shown in Fig. 2(b). After folding different parts are locked in place using snap-in features in the composite sheet without the need for any fasteners. The folding of the SCM sheet also increases its bending stiffness and reduces deformation under load.

The claws of the gripper are also realized based on the SCM structures. The stretchable fabric integrated inside the SCM structure of the claws provides the antagonistic force for returning the claws, clutches, and Sarrus linkage to the initial open position once clutches are turned OFF. A Hall effect sensor in each claw measures the claw angle for activating the locking mechanism at a fully closed state.

The full gripper, including the battery and electronics, weighs 150 g and can hold up to 4 kg in quasi-static state. Given the low energy consumption of the clutches and control circuit, a

650-mWh battery can keep two grippers engaged and an UAV perched, for 140 min.

III. PASSIVE DYNAMIC GRASP BY RECYCLING IMPACT ENERGY

The inertial forces of the claws are the dominant factor in the dynamic response of a passive dynamic gripper. Therefore, the acceleration of the claws determines the mechanics of the gripper. In our design, the motion of the linkage and claws are coupled through soft tendons; see Fig. 3. We use the stiffness of these tendons to adjust the acceleration of the claws for effective energy transfer without object reflection.

A. Soft Coupling for Smooth Energy Transfer

To study the role of tendon stiffness on the mechanics of impact, we use a pendulum setup presented in Fig. 3(a). The dynamic response of the gripper is captured at 2000 frames per second using a high-speed camera (Miro eX4/Phantom). The sequence of snapshots in Fig. 3(c) presents an example of a successful grasp. The recordings were processed to extract the position and velocity of the impacting object and different parts of the gripper. The ground reaction force is recorded at 2000 samples per second using a loadcell (KTOYO-333FDX) that connects the gripper to the ground.

The equivalent mechanical model of our gripper is presented in Fig. 3(b). The stiffness of the tendon in this system is the parameter that we use to control the mechanics of the gripper. To perform a parametric study, we used the same gripper (fixed tendon) and changed the stiffness of the tendon puller [see Fig. 3(a)] to adjust the coupling between the ankle linkage and the claws. We used 1–4 sheets of 0.15-mm-thick Manganese spring to increase the stiffness of the tendon puller in four increments. We also used a 3-mm-thick acrylic sheet as a relatively rigid tendon puller. The change in the stiffness of the tendon significantly affects the mechanics of the gripper and its response to impact, as presented in Fig. 4(a)–(d). The impacting object in these experiments weighs 300 g and its impact velocity is 2 m/s.

For a specific impact condition (mass and velocity), there is an optimum tendon stiffness (case k_{t-2} in Fig. 4) that results in complete transfer of energy from the impacting object to the Sarrus linkage, which leaves the object at rest after the energy transfer. In this case, the Sarrus linkage and claws arrive at their fully folded state at the same time [see Fig. 4(b) and (d)], allowing the locking of the claws with no slack in the tendon.

When the motion of the claw is coupled to the motion of the linkage with a stiffer tendon (k_{t-3} – k_{t-5}), the object is reflected from the surface of the gripper without fully transferring its kinetic energy. On the other hand, for the case in which the tendon is softer (case k_{t-1}), the Sarrus linkage arrives at the stopper before complete kinetic energy transfer; see Fig. 4(b). This results in a secondary impact and reflection of the object from the stopper at the base of the Sarrus linkage; see Fig. 4(c). In this case, the object is reflected at a high velocity before the claws of the gripper are fully closed; see Fig. 4(a).

Comparing the final configuration of the gripper with different values for tendon stiffness in Fig. 4(e) demonstrates the

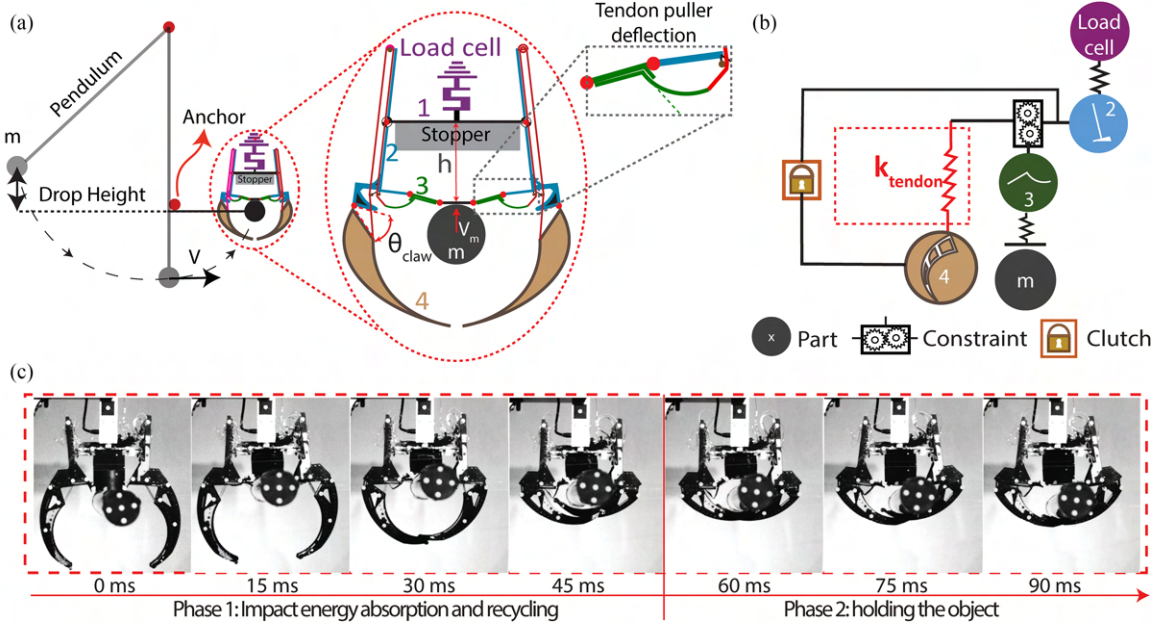


Fig. 3. (a) Experiment setup to study the dynamic response of the passive dynamic gripper. Deflection in the tendon puller allows a soft coupling between the ankle linkage and claws. (b) Equivalent model of the gripper highlighting the soft coupling. (c) Snapshots of a passive dynamic grasp. In phase 1, the object transfers its kinetic energy to the gripper resulting in claw closure. Once the claws are closed, electroadhesive clutches are engaged to lock the configuration in the holding phase.

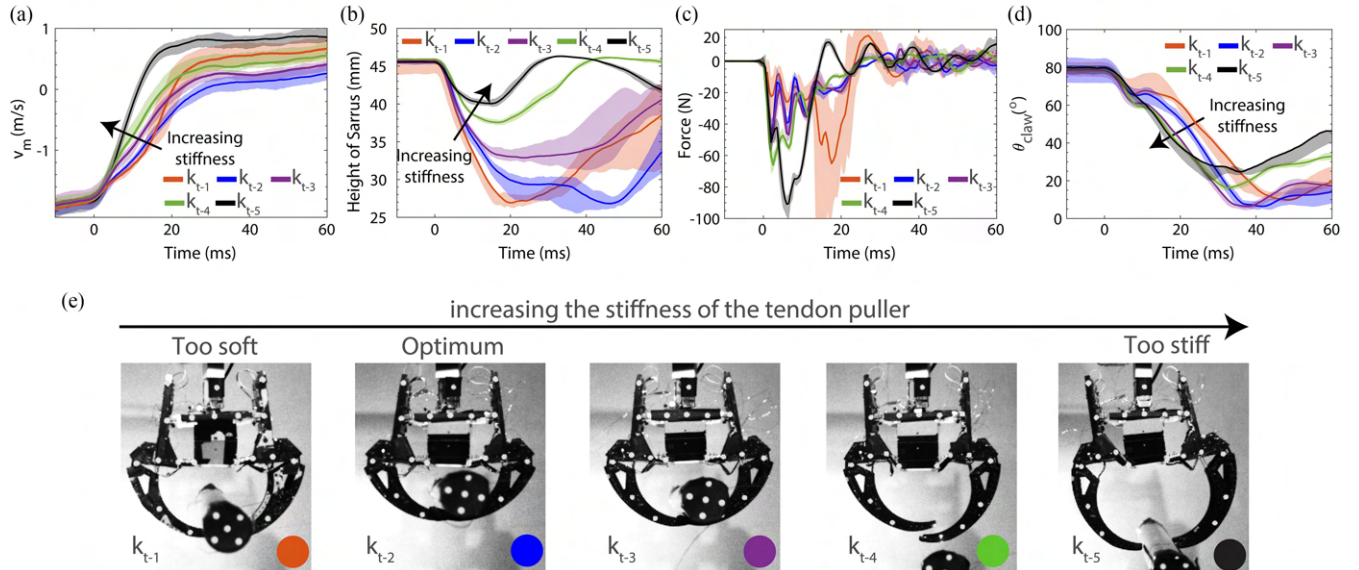


Fig. 4. Effect of tendon stiffness on the mechanics of impact. (a) Rate of change in the velocity of the impacting object increases with tendon stiffness. For the softest tendon (k_{t-1}), the inflation point indicates a secondary impact at the stopper (as the ankle linkage reaches its fully folded state). (b) Height of the Sarrus linkage shows that for stiff tendons, k_{t-3} – k_{t-5} , linkage does not fully fold, due to object reflection. For softer tendons, the motion faces less resistance allowing the mechanism to move faster and further. (c) Impact force increases with the tendon stiffness due to a stronger coupling between the linkage and the claws. For the softest tendon (k_{t-1}), the peak corresponds to object reflection from the stopper. (d) Initially, the claw accelerates faster for stiffer tendons (k_{t-4} and k_{t-5}). But as the Sarrus linkage stops folding, claws slow down and do not fully close. For the softest tendon (k_{t-1}), the rate of energy transfer is too slow, and the claw does not fully close before reflection off of the ankle linkage stopper. (e) Final configuration of the gripper indicates that for the impact conditions in this experiment, tendon stiffness corresponding to the second case results in the best performance. The error bands contain the results of ten repetitions. The supplementary video presents examples of impact for grippers with different tendon stiffness.

importance of the tendon stiffness in effective closure of the gripper. In the first case (soft tendon— k_{t-1}), the slow rate of energy transfer resulted in the reflection of the object from the stopper before complete claw closure and in turn the loose grasp. On the other hand, for the cases with excessively strong coupling

(k_{t-3} – k_{t-5}), the reflection of the object after first contact with the gripper prevented complete transfer of the kinetic energy resulting in increasingly looser grasp as tendons become stiffer. For the impact condition studied in this experiment, the second lowest tendon stiffness (k_{t-2}) resulted in the best performance.

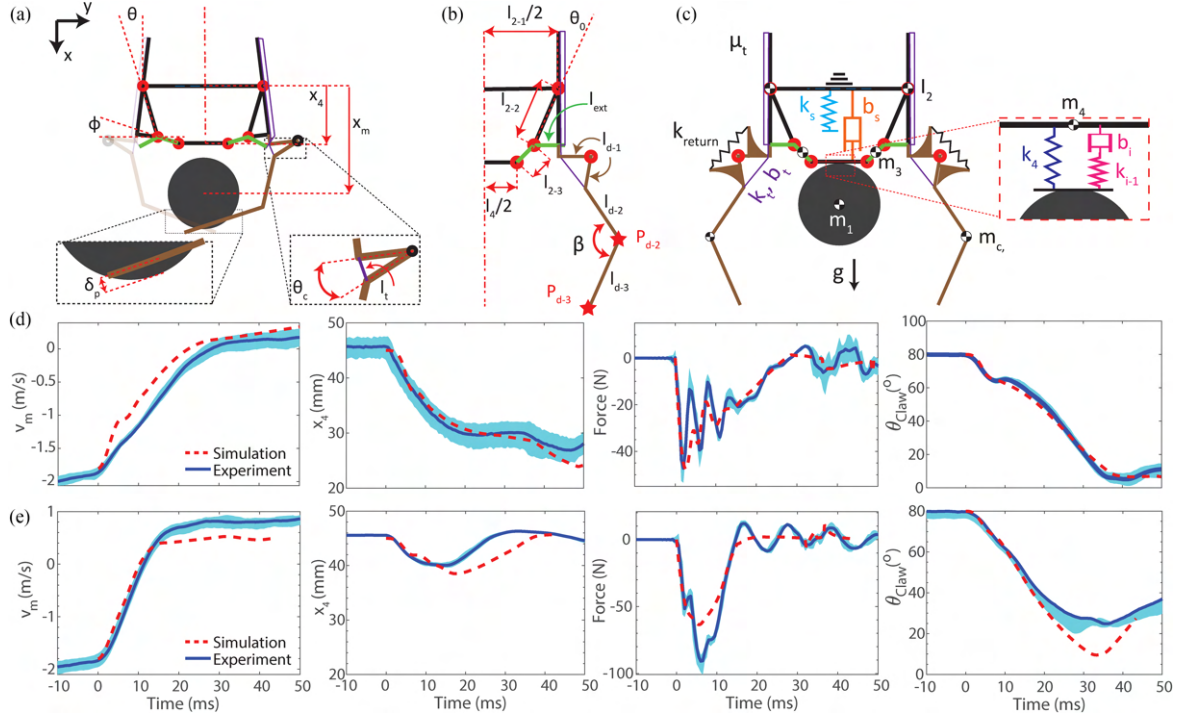


Fig. 5. Dynamic model of the gripper. (a) Kinematic variables of the model. (b) Kinematic design parameters. (c) Dynamic model parameters. (d) Simulation and experiment results for grippers with tendon stiffness k_{t-2} and (e) k_{t-5} . The simulation results capture the main features of the dynamic response and the effect of the tendon stiffness on the mechanics of the impact.

In this case, the kinetic energy is completely transferred to the claws and both the Sarrus linkage and the claws reach fully folded state at the same time and when the object is at rest, which results in the tight holding state presented in Fig. 4(e).

Depending on the stiffness of the tendon, the passive dynamic gripper can perform successful grasp for a range of impacting masses and velocities. In the next section, we present a dynamic model of the gripper that allows us to determine the range of impact conditions leading to a successful grasp, based on tendon stiffness.

B. Dynamics Model of the Gripper

We developed a dynamic model for the gripper using the Lagrangian approach to study the effect of tendon stiffness on the mechanics of the gripper. The independent kinematic variables in the model are: the position of the impacting object (x_m), the folding angle of the Sarrus linkage (φ), and the claw angle (θ_C), presented in Fig. 5(a). The position of the other links (θ , x_4) are calculated using the following kinematic constraints:

$$\theta = \sin^{-1} \left(\frac{(l_3 \cos(\varphi_0) - l_3 \cos(\varphi) + l_2 \sin(\theta_0))}{l_2} \right) \quad (1)$$

$$x_4 = l_2 \cos(\theta) + l_3 \sin(\varphi) \quad (2)$$

where l_i represents the length of the corresponding link in Fig. 5(b). The length of the tendon (l_t) at the claw joint is calculated as

$$l_t = 2l_{d-1} \sin \left(\frac{\theta_C}{2} \right). \quad (3)$$

In the model, the claw is simplified and represented by two lines; represented by l_{d-2} and l_{d-3} in Fig. 5(b). The interaction of the object with the claw is modeled by a spring acting against the indentation of the claw into the object. Indentation depth, δ_P , is calculated as the distance between a line and a circle

$$\delta_P = r_m - \frac{|(y_{d-3} - y_{d-2})x_1 + x_{d-3}y_{d-2} - y_{d-3}x_{d-2}|}{\sqrt{(y_{d-3} - y_{d-2})^2 + (x_{d-3} - x_{d-2})^2}} \quad (4)$$

where r_m is the diameter of the impacting object. The other variables in this equation are the coordinates of the points that define the segment of the claw in contact with the object [P_{d-2} , P_{d-3} in Fig. 5(b)]. Tendon elongation, δl_t , is calculated as

$$\delta l_t = 2l_{ext} \sin \left(\frac{\phi - \phi_0 - \theta + \theta_0}{2} \right) - l_t + l_{t-0}. \quad (5)$$

The Lagrangian of the system (L) is

$$L = T - U. \quad (6)$$

where T represents the kinetic energy of the system and is calculated as

$$T = \frac{1}{2} \left(m_m v_m^2 + m_4 v_4^2 + 2m_3 v_3^2 + 2m_c v_c^2 + 2I_3 \dot{\phi}^2 + 2I_2 \dot{\theta}^2 + 2I_c (\dot{\theta}_c - \dot{\theta}^2)^2 \right) \quad (7)$$

where m_i , v_i , I_i , and $\dot{\theta}_i$ represent mass, velocity, moment of inertia, and angular velocity of the i th link. The geometric parameters and inertial properties of each link in (7) are measured directly. The potential energy of the system (U) is

calculated as

$$\begin{aligned} U = & m_m x_m g - m_4 x_4 g - m_3 x_3 g - m_c x_c g \\ & + \frac{1}{2} \left(k_4 (x_4 - (x_m - r_m))^2 + k_t (\delta l_t)^2 + k_C (\delta_P)^2 \right. \\ & \left. + k_L (\theta_C - \theta_{C-L})^2 + k_s (x_s - x_4)^2 \right) \end{aligned} \quad (8)$$

where $\langle \rangle$ represents an operator that returns zero for negative values; x_i in this equation represents the position of each object along the vertical axis, as defined in Fig. 5(a); and k_4 , k_t , k_c , k_L , and k_s , respectively, represent the spring constants of link 4 at the contact point with the object, tendon spring constant, claw stiffness at the contact point with the object, stiffness of the claw joint when it is locked, and linkage stopper spring constant, respectively.

The viscous dissipation terms are included in the model using Rayleigh dissipation function as follows:

$$\begin{aligned} R = & \frac{1}{2} b_s v_4^2 + \frac{1}{2} b_t \dot{\delta l}_t^2, & \delta l_t > 0 \\ R = & \frac{1}{2} b_s v_4^2, & \delta l_t < 0 \end{aligned} \quad (9)$$

where b_s and b_t represent damping in the Sarrus linkage and tendon, respectively. The spring constants in (8) and damping constants in (9) are lumped representations of different elements in the gripper, some of which are significant only in during impact. As a result, direct quasi-static measurement of these components is not feasible. We used the experiment results of passive dynamic grasp corresponding to case k_2 and k_5 in Fig. 4 to tune these parameters.

The remaining elements of the model are accounted for as external forces in the Euler–Lagrange (10) and (11). The following are the equations of motion for the impacting object and Sarrus linkage, respectively

$$\frac{d}{dt} \left(\frac{\partial L}{\partial \dot{x}_1} \right) - \frac{\partial L}{\partial x_1} + \frac{\partial R}{\partial \dot{x}_1} = F_{i-1} \quad (10)$$

$$\frac{d}{dt} \left(\frac{\partial L}{\partial \dot{\varphi}} \right) - \frac{\partial L}{\partial \varphi} + \frac{\partial R}{\partial \dot{\varphi}} = -F_{i-1} \frac{dx_2}{d\varphi} - \mu_t F_t \frac{dl_t}{d\varphi} \quad (11)$$

where F_{i-1} represents the force in the spring damper branch of the contact model for object and gripper; see Fig. 5(c). The Force in this branch is calculated as

$$\begin{aligned} \dot{F}_{i-1} = & \frac{-k_{i-1} F_{i-1}}{b_{i-1}} + k_{i-1} (\dot{x}_2 - \dot{x}_1), & x_1 - r < x_4 \\ \dot{F}_{i-1} = & \frac{-k_{i-1} F_{i-1}}{b_{i-1}}, & x_1 - r > x_4. \end{aligned} \quad (12)$$

The second term on the right-hand side of (11) accounts for the dissipation due to the frictional losses in the tendon in its interaction with the pulleys. F_t in this term is the tendon tension and μ_t is the lumped friction coefficient of all pulleys. The friction coefficient was measured to be 0.47 (by pulling different weights through the pulley system in quasi-static condition). For a given mass, the higher bound of impact velocity for a successful grasp can be increased by using stiffer tendons. The lower bound, however, is limited by the energy losses. The most significant sources of energy loss in the current implementation of the

gripper are the frictional losses. In the future, we will reduce these losses and broaden the application range of the gripper by fixing the tendon pulleys to the structure using bearings.

Finally, the equation of motion for the claw is

$$\frac{d}{dt} \left(\frac{\partial L}{\partial \dot{\theta}_C} \right) - \frac{\partial L}{\partial \theta_C} + \frac{\partial R}{\partial \dot{\theta}_C} = \tau_C - \mu F_t \frac{dl_t}{d\theta_C} \quad (13)$$

where τ_C represents the force applied by the return spring (stretchable fabric) to the claws. This term is added as an external force (rather than a term in the potential energy) since it has a nonlinear relation with the joint angle. This parameter was characterized in quasi-static state. We solved (1)–(13) using MATLAB ODE solver to simulate the dynamic response of the gripper in different impact conditions.

Fig. 5(d) and (e) presents simulation results for a gripper with two different tendon stiffness, corresponding to k_{t-2} , k_{t-5} in Fig. 4. The predicted object velocity, Sarrus linkage height, ground reaction force, and the claw angle closely match with the experiment results. The simulation predicts smooth energy transfer for the gripper with lower tendon stiffness (k_{t-2}) and object reflection without complete energy transfer for the stiffer tendon (k_{t-5}). In the next section, we use our dynamic model to predict the range of impact velocities and masses that result in a successful grasp for grippers with different tendon stiffness.

C. Impact Conditions for a Successful Grasp

By running the simulation in different impact conditions, mass, and velocity, we can find the range of conditions that result in a successful grasp. We simulated the impact with masses between 200 and 900 g, with 50-g increments. We selected the velocity range according to the selected range for the impacting mass.

To rate the performance of the gripper in each impact condition, we considered the following three variables: the minimum folding height of the Sarrus linkage (h_{min}), the velocity of the object at the stopper ($V_{at\ stopper}$), and the locking angle of the claws ($\theta_{Claw-lock}$). Fig. 6(a)–(c) presents the value of these three parameters (from simulation) for a gripper with tendon stiffness corresponding to case k_{t-2} in Fig. 4.

The minimum height of the Sarrus linkage determines if the kinetic energy and momentum of the impacting object were large enough in each case to sufficiently fold the linkage, and in turn, pull the digital tendons. The blue shaded area in Fig. 6(a) represents acceptable range according to this variable.

Ideally, the object arrives at the stopper of the gripper with a very small velocity and rests steady, while the electro-adhesive clutches are engaged. We considered an impact condition to be admissible if the secondary impact has a velocity smaller than 0.3 m/s. The green shaded area in Fig. 6(b) represents the valid condition according to this variable. The acceptable velocity for the secondary impact can be modified depending on the admissible impact force and reflection velocity (the value assigned here is to show the trend).

Finally, the most important variable to assess the performance is the locking angle of the claw ($\theta_{Claw-lock}$). The red shaded area in Fig. 6(c) is the region in which the locking angle of the claws is

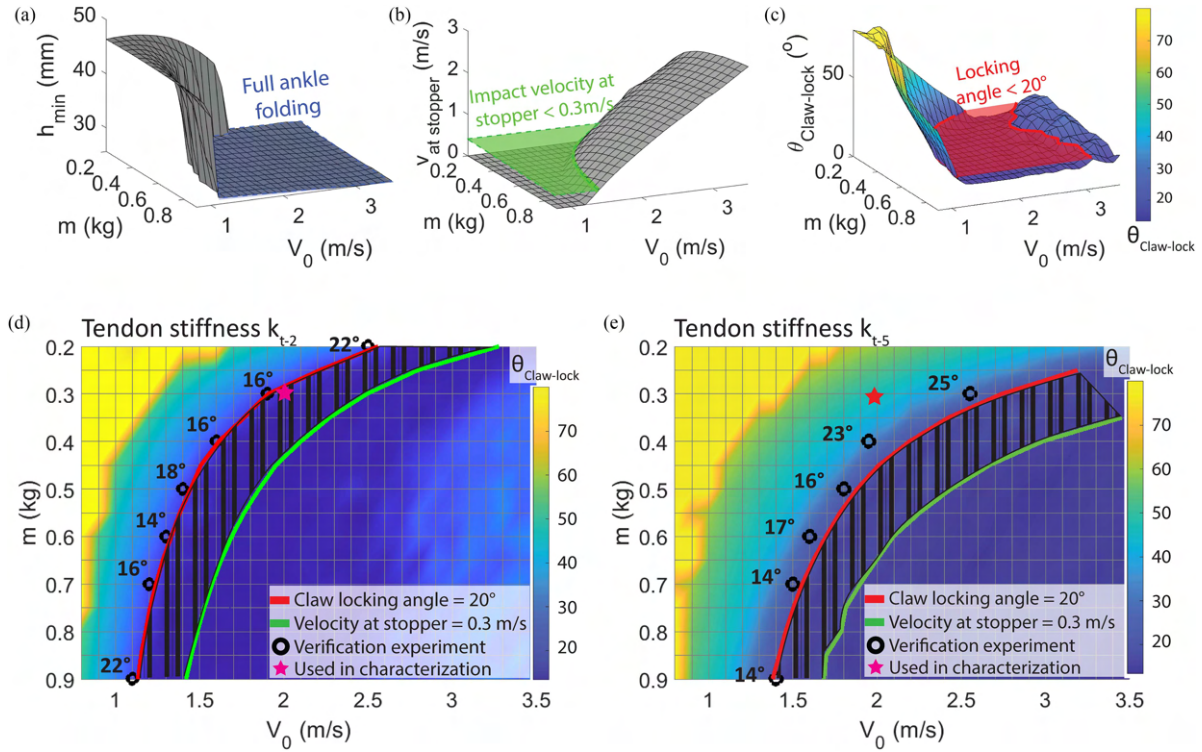


Fig. 6. Gripper performance in different impact conditions. (a) Minimum height of the Sarrus linkage after impact and during claw closure. (b) Velocity of the object at the stopper of the Sarrus linkage. (c) Locked position of the claw. Results in (a)–(c) correspond to tendon stiffness k_{t-2} . (d) Application range of the passive dynamic gripper (hatched area) for case k_{t-2} and (e) case k_{t-5} . The red line in these figures indicate the impact conditions leading to locking angle of 20° for the claw. Points to the right side of this line result in smaller angle and successful grasp. The green line indicates the conditions leading to secondary impact with 0.3 m/s (which was chosen as the maximum acceptable velocity at the stopper). Impact conditions to the left side of this line are acceptable. The area between the green and red lines indicate the acceptable impact conditions for the gripper. As the tendon becomes stiffer, this range shifts to the right. The model prediction was verified by conducting a series of experiments with different impact conditions along the red line. In all experiments (for both tendon stiffness), the gripper successfully closed and held the object with an angle close to the predicted 20° and without a secondary impact.

smaller than 20° , resulting in overlapped claws and a successful grasp.

The intersection of the three shaded areas in Fig. 6(a)–(c) determines the admissible range of impact conditions for a successful grasp. This range for the case k_{t-2} is presented in Fig. 6(d), the hatched area. To verify the simulation results, multiple conditions along the 20° locking angle curve in Fig. 6(d) were tested. The gripper in all cases (three repetitions for each case) successfully grasped the object with no secondary impact. The final claw angle, $\theta_{\text{Claw-lock}}$, in these experiments are reported in the plot and matches closely with the expected value of 20° .

Increasing the tendon stiffness shifts the admissible impact range to the right as seen in Fig. 6(e), corresponding to a gripper of case k_{t-5} in Fig. 4. The shift to the right for the stiffer tendon indicates that heavier objects and faster impact velocities are required for successful grasp as the coupling between the linkage and claws become stronger. The results presented in Fig. 6(d) and (e) can be used to choose a tendon stiffness based on the impact conditions.

D. Tendon Stiffness as a Control Parameter

In this article, we primarily treat the tendon stiffness as a design parameter. However, to show the feasibility of using the

stiffness as a control parameter, we made a version of the gripper with variable stiffness tendons; see Fig. 7. This version of the gripper is made at 0.7 scale of the larger gripper as shown in Fig. 7(a) (to show the scalability of the design and manufacturing frameworks). To control the stiffness of the tendon, we repurposed half of the electroadhesive clutching pairs as presented in Fig. 7(b). The bottom half of the electroadhesive clutch stack (claw side of the tendon) is used to lock the digital tendons and is identical to the design presented in Fig. 2. On the side of the tendon puller, however, stationary clutches are removed. The tendon on this side is cut into two pieces that are connected through a stretchable fabric layer; see Fig. 7(b). The two sides of the tendon are connected to a clutch pair that we refer to as stiffness modulating clutch (SM clutch). When SM clutches are disengaged, the tendon stiffness is the same as the stiffness of the stretchable fabric. When SM clutches are activated, the force is transferred through the clutch pair between the two sides of the tendon and the stretchable fabric is bypassed, resulting in a higher tendon stiffness.

To confirm the effectiveness of this design for controlling the dynamic response of the gripper, we studied the interaction of an impacting mass (200 g) at two impact velocities. At lower velocity (1.5 m/s), the gripper has a better performance when the SM clutches are disengaged and the stretchable fabric is in series with the tendon. In this case, the elongation

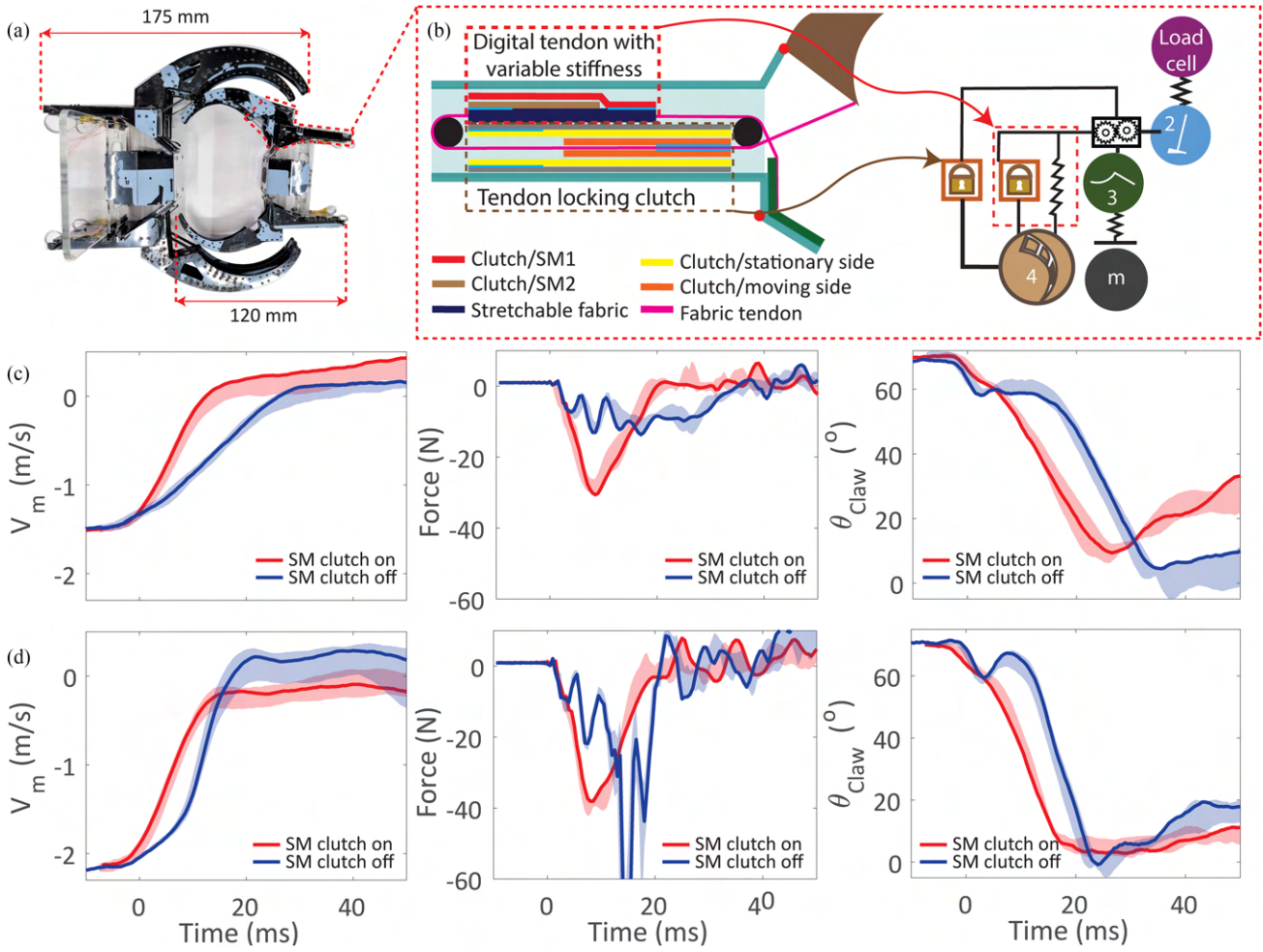


Fig. 7. Passive dynamic gripper with variable stiffness tendons. (a) Scaled down version of the gripper has variable stiffness tendon. (b) Half of the electrostatic clutch pairs (SM clutch pairs) are repurposed to engage and disengage a stretchable fabric in series with the tendon. (c) Dynamic response of the gripper interacting with a 200-g object with 1.5-m/s velocity. In this case, when the SM clutch pairs are disengaged and the tendon is soft, the gripper has a better performance. (d) Dynamic response of the gripper interacting with a 200-g object with 2-m/s velocity. In this case, gripper has a better performance when SM clutch pairs are engaged and the tendon has a higher stiffness. Error bands contain the results from five repetitions.

of the stretchable fabric allows slower energy transfer within a longer interaction period that results in a smaller final angle for the claws; see Fig. 7(c). When SM clutches are activated at a lower impact velocity, the object gets reflected with a relatively large impact force and the Sarrus linkage does not fully fold. This results in slack in the tendon when the tendon locking clutch pairs are activated. As a result, in this case, the final claw angle is significantly larger, and in our experiments, the object slipped out in 3 out of 5 repetitions. The trends are reversed at impact velocity of 2 m/s; see Fig. 7(d). In this case, the soft tendon (SM clutches OFF) fails to fully transfer the energy to the claws within the range of motion of the Sarrus linkage. As a result, the object is reflected with a large impact force from the stopper. At high impact velocity, the stiff tendon (SM clutches ON) results in a better performance in terms of outgoing velocity, maximum impact force, and closure angle. Moreover, better energy transfer to the claws results in almost 25% faster claw closure. This feasibility study demonstrates the possibility

of using electroadhesive clutches for modulating the mechanics of the gripper depending on the velocity of the impacting objects.

IV. GRIPPER'S RESILIENCE AGAINST OFF-CENTER IMPACTS

The compliance of the links in the SCM mechanism allows it to automatically align with the impacting object in the case of an offset loading, as presented in Fig. 8. This allows successful grasp in the presence of positioning errors. We verified the possibility of a successful grasp with different offset distance, in the range of 0–4 cm [see Fig. 8(c)], by changing the length of the pendulum in the experiment setup presented in Fig. 3. The rotation angle of the Sarrus linkage increases with the offset as presented in Fig. 8(d), which indicates self-alignment of the gripper. During this alignment process, the 3-D-printed guide pushes the object toward the center. The combined effect of the rotation of the ankle linkage and the force from the 3-D-printed guide results in a successful grasp in all cases. As

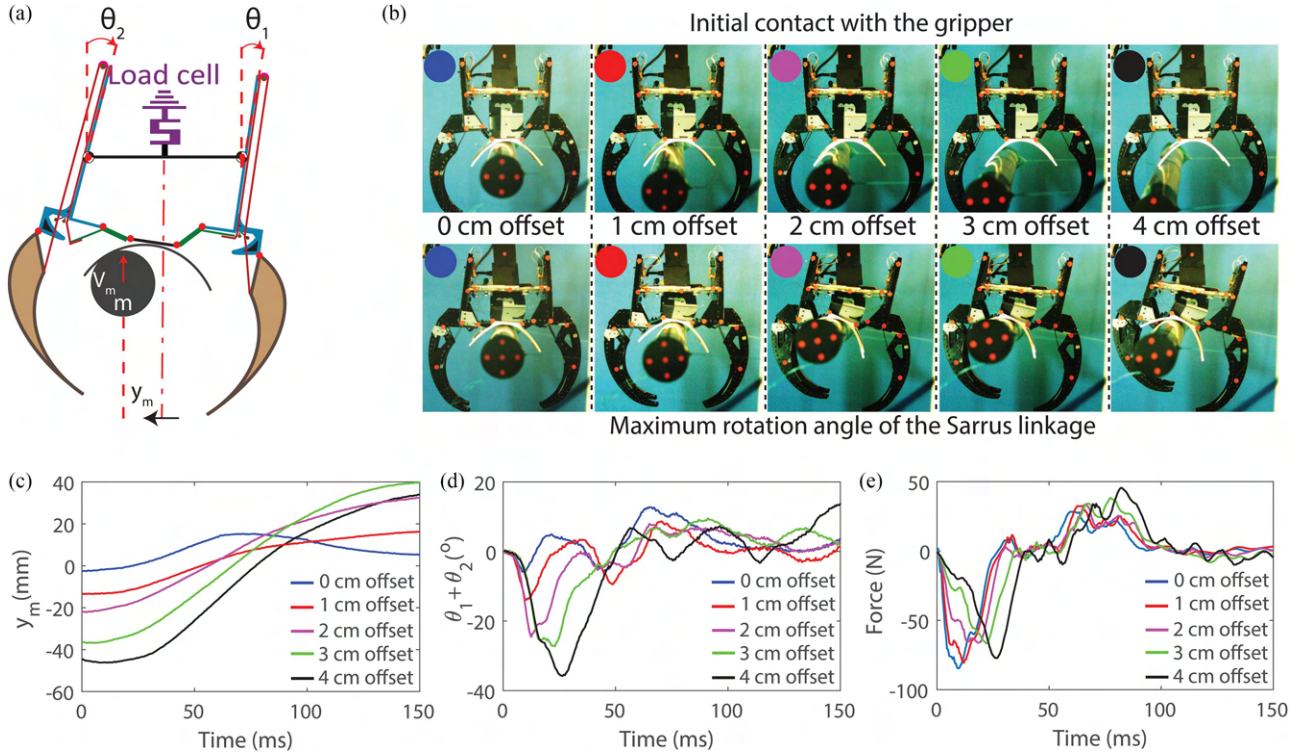


Fig. 8. Dynamic response of the passive dynamic gripper to off-center impact. (a) Schematic of the experiment. (b) Snapshots of the interaction of the gripper with an off-center impacting object. (c) Lateral position of the object. (d) Rotation of the linkage. (e) Reaction force at the base of the Sarrus linkage.

the offset increases, the object bounces more aggressively in the y -direction; see Fig. 8(c). This results in relatively large pullout forces with the maximum of 45 N [see Fig. 8(e)] for the offset of 40 mm. The gripper resisted this pullout force in all cases and successfully held the object. The resilience against off-center impact ensures reliable perching in the presence of relatively large positioning errors in the UAV experiments.

V. AERIAL PERCHING AND GRASPING EXPERIMENTS

Impact is an inseparable part of physical interaction for aerial robots. It can be caused by deviations from a planned path due to aerodynamic disturbances or by an intended dynamic approach for perching in quasi-statically unstable orientations. Our bioinspired passive dynamic gripper is designed to perform perching and grasping tasks in the presence of such impact loading. Our gripper smoothly absorbs the impact energy, which prevents the UAV from bouncing off of the target, and utilizes the absorbed energy for automatic claw closure. Driving the motion of the claws by using the impact energy simplifies the control and eliminates the problem of coordinating the motion of the gripper and the UAV. All the control that is required for perching using the passive dynamic foot is positioning the UAV above the target and simply turning OFF the propellers for free falling.

For our aerial perching and grasping experiments, we equip a DJI F450 UAV with two grippers each with 40-N loading capacity; see Fig. 9(a). The loading capacity of the gripper was characterized using an Instron Universal testing system

by pulling cylindrical objects with diameters of 35, 45, and 55 mm [experiment results for 55-mm object is presented in Fig. 9(b)].

The position of the UAV is controlled using a trajectory-tracking controller based on a back-stepping control method [30]. This controller has a cascaded structure that consists of an outer position controller and an inner angular rate controller. The position controller receives continuous position and yaw trajectory information from the trajectory planner and provides the desired thrust and angular rate as outputs. Then, the inner angular rate controller follows the desired angular velocity given by the position controller based on PID feedback control. This cascaded structure with thrust/angular rate control is generally utilized in conventional multirotor UAVs. Therefore, without loss of generality, the scenarios implemented in this research can be realized with other conventional UAVs.

The UAV is equipped with Pixhawk 4.0 as a flight control unit (FCU) and RaspberryPi 3B+ as an onboard computer, which implemented the back-stepping controller and trajectory planner. An external motion capture system, Optitrack, is used to provide UAV position and orientation information at 120 Hz. The position and orientation information are fused with inertial measurement unit (IMU) sensor information from Pixhawk via an extended Kalman filter (EKF).

The controller positions the UAV on top of the target and turns OFF all the propellers allowing the UAV to free fall onto the target, as presented in Fig. 9(c) and supplementary video. Once hitting the target, the impact force causes the grippers to automatically close around the perch and electroadhesive

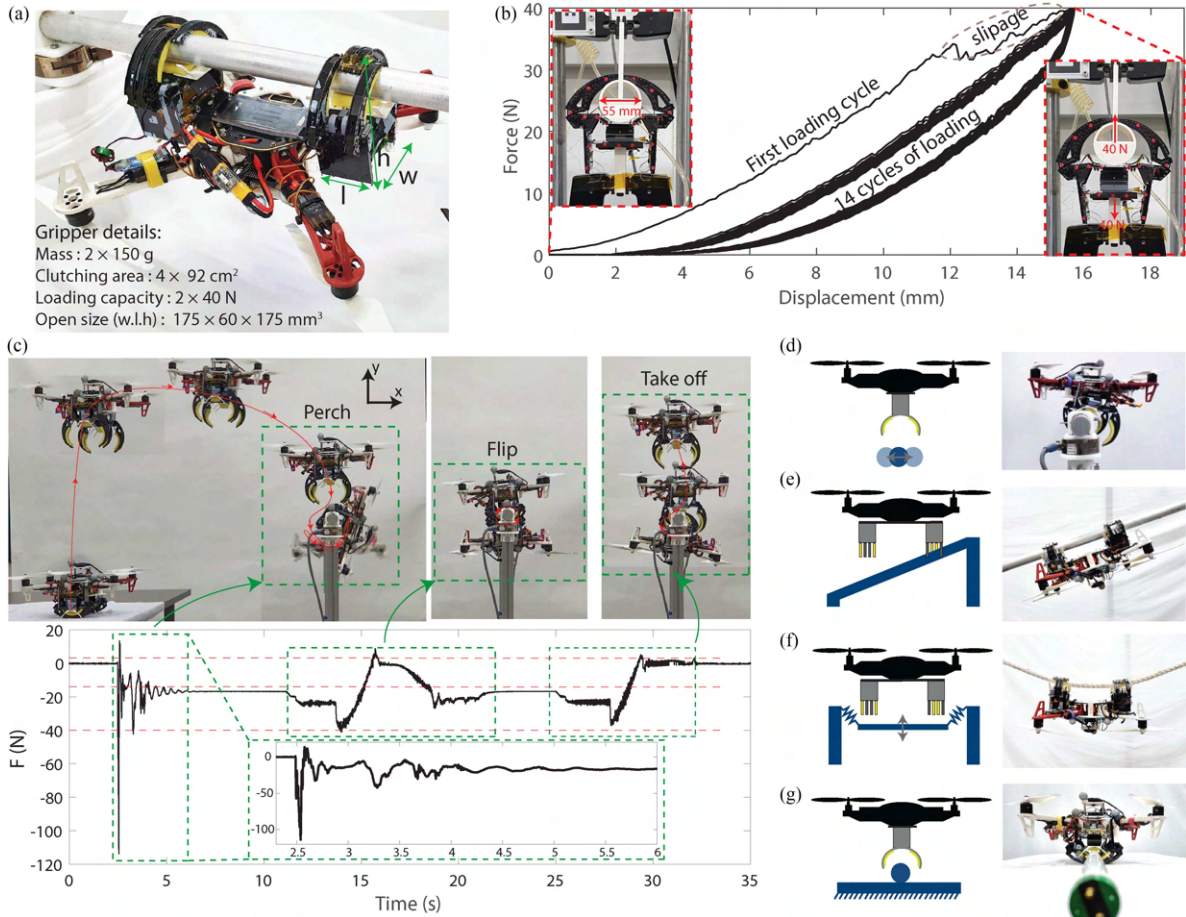


Fig. 9. Aerial perching and grasping with passive dynamic feet. (a) Two passive dynamic grippers with the combined loading capacity of 80 N are used as the feet of the UAV. (b) Quasi-static loading of the gripper. Gripper holds the object against pulling force of 40 N. Due to slack in the tendon and misalignment between clutch pairs, clutches slide slightly in the first loading cycle (in the highlighted region). In the consequent cycles, there is no additional sliding, and the force–displacement profile shows a negligible change in 14 cycles. (c) Perch and release experiment. Gripper engages automatically upon impact after UAV free falls on the perch. Perching on challenging targets is possible without any modification to the UAV controller. (d) Perching in the presence of positioning error. (e) Perching on an inclined bar (a quasistatically unstable condition). (f) Perching on an elastic beam (rope). (g) Closure of the claws in response to ground reaction forces allows picking up objects from flat surfaces. Here, the example of grasping a fragile light tube is presented. For videos, refer to supplementary materials.

clutches lock the mechanism in this closed configuration, while the UAV rotates toward its stable equilibrium point under the perch. Dynamic loads during this landing rotation and the reverse release rotation, result in around 40-N pullout force (roughly twice the weight of the UAV); see Fig. 9(c). The two feet have a combined loading capacity of 80 N. This loading capacity provides a safety factor of 2 and guarantees the reliability of the dynamic perching maneuver.

With the weight of the drone helping with the closure of the passive dynamic grippers in the perching experiments, free falling from a wide range of heights (1–15 cm) results in successful perching. As discussed in the previous section, the gripper is also resilient against off-center impacts, up to 4 cm. So, in UAV perching experiments, a wide range of positioning errors is admissible; see Fig. 9(d) and supplementary video.

Automatic closure of the passive dynamic grippers allows the execution of complex tasks, such as perching on an inclined target, with no additional control effort and no trajectory modification, as presented in Fig. 9(e) and supplementary video. We successfully perched on a 35-mm diameter rod with inclinations

of 0°, 5°, 10°, 15°, and 20°. At 15° and 20° inclination, the drone slides along the rod but eventually the friction from the foam pads that cover the claws stops the sliding motion.

Another example of a challenging scenario is perching on an unstable target, such as a rope. Contact between the UAV and the rope can cause significant displacement of the rope. Perching using an active gripper would require following this trajectory during the closure time of the gripper. In the case of the passive gripper, however, perching is possible without any modifications in the control strategy and by simply free falling, as presented in Fig. 9(f) and supplementary video.

The claws of the passive dynamic gripper are designed to close in response to ground reaction forces when the UAV lands on a flat surface. This feature is utilized for picking up objects with diameters ranging from 20 to 50 mm. For small objects (20–30 mm in diameter), after the closure of the gripper, the ground reaction force does not pass through the object, allowing the gripper to safely pick up and transport fragile objects. An example of grasping a fragile light-tube with diameter of 20 mm is presented in Fig. 9(g) and the supplementary video.

The passive dynamic grippers that are used in the drone experiments have the following shortcomings: fixed tendon stiffness (hence fixed gripper mechanics), fixed claw shape, and lack of squeezing force after claw closure. Fixed tendon stiffness limits the range of impact velocities that would result in a successful grasp. Grippers with adjustable tendon stiffness (introduced in Section IV) can address this shortcoming in the future. The variable stiffness tendon will allow us to control the mechanics of the drone foot based on the approach velocity for optimum and smooth impact energy transfer without object reflection.

Fixed shape of the claws is another limitation of the current device that prevents conformation to the shape of the object. Due to this limitation, in our experiments, we were limited to cylindrical objects with circular or square cross sections. In the future, this limitation can be overcome by adding underactuated tendon-driven degrees of freedom in the claws. These degrees of freedom can be driven by the same tendon that is currently used to drive the joint at the base of each claw.

Finally, our gripper cannot exert squeezing force after closure. The lack of squeezing force prevents steady perching on top of a cylinder [see Fig. 9(c)] and is the reason for the sliding motion of the drone when perching on inclined cylinders [see Fig. 9(e)]. In the future, active (or spring-loaded) elements can be integrated in the gripper to provide squeezing force after claw closure. We did not include such elements in the current device since our focus was on recycling the impact energy in a passive dynamic gripper.

Despite its limitation, the passive dynamic gripper was effective as the drone foot in all the perching and grasping scenarios studied here. The simple control sequence for engaging the gripper, low energy consumption, and scalability of the design makes the presented UAV foot a viable option for UAVs of different sizes and designs.

VI. CONCLUSION

In this article, we presented a bioinspired passive dynamic gripper that utilized the impact energy for driving its claws. Successful energy transfer during impact required a delicate balance between the mechanics of the gripper and impact conditions (mass and velocity). In our passive dynamic gripper, we coupled the motion of the ankle linkage with the motion of the claws through elastic tendons and used the stiffness of this tendon to tune the mechanics of the gripper. By simulating the dynamic response of the gripper in different conditions, we estimated the range of mass and velocity that results in a successful grasp and demonstrated how the stiffness of the tendon can be used as a design parameter to change the application range of the gripper.

For locking the configuration of our passive dynamic gripper after closure, we used a tendon locking mechanism based on electroadhesive clutches. The compact design of this locking mechanism allows its integration at close proximity of the claws for preventing any recoil or undesired opening of the claw due to elongation in the digital tendons.

We presented a scaled down version of the gripper with variable stiffness tendon in which electroadhesive clutches were used to actively control the stiffness of the tendon between two

values. We used the variable stiffness of the tendon to adjust the mechanics of the gripper for successful grasp in two different conditions.

To show the effectiveness of our passive dynamic gripper, we used it as an UAV foot and performed a series of dynamic perching and grasping tasks. The automatic closure of the feet allowed performing complex perching tasks with little control effort. In the future, we will improve the capabilities of our gripper by adding active elements that would allow tighter grasp for holding the UAV above the rod. The methods for the passive dynamic grasp that were developed in this article will be applicable in such a gripper for smooth and fast interactions by recycling the impact energy. We will also further develop the variable stiffness tendons with multiple stiffness settings for effective energy recycling depending on the approach speed of the UAV. Finally, we will take the UAV experiments out of the controlled lab environment and perform similar perch and grasp tasks in the presence of environmental disturbances.

REFERENCES

- [1] W. R. Roderick, D. D. Chin, M. R. Cutkosky, and D. Lentink, “Birds land reliably on complex surfaces by adapting their foot-surface interactions upon contact,” *Elife*, vol. 8, 2019, Art. no. e46415, doi: [10.7554/eLife.46415](https://doi.org/10.7554/eLife.46415).
- [2] A. A. Biewener, “Getting to grips with how birds land stably on complex surfaces,” *Nature*, vol. 574, pp. 180–181, 2019, doi: [10.1038/d41586-019-02959-w](https://doi.org/10.1038/d41586-019-02959-w).
- [3] F. Gill and R. O. Prum, “Basic characters of birds,” in *Ornithology*, 4th ed. San Francisco, CA, USA: Freeman, 2019, pp. 53–62.
- [4] P. M. Galton and J. D. Shepherd, “Experimental analysis of perching in the European Starling (*Sturnus vulgaris*: Passeriformes; Passeres), and the automatic perching mechanism of birds,” *J. Exp. Zool. A, Ecological Genet. Physiol.*, vol. 317, no. 4, pp. 205–215, 2012, doi: [10.1002/jez.1714](https://doi.org/10.1002/jez.1714).
- [5] A. B. Ward, P. D. Weigl, and R. M. Conroy, “Functional morphology of raptor hindlimbs: Implications for resource partitioning,” *Auk*, vol. 119, no. 4, pp. 1052–1063, 2002, doi: [10.1093/auk/119.4.1052](https://doi.org/10.1093/auk/119.4.1052).
- [6] T. H. Quinn and J. J. Baumel, “The digital tendon locking mechanism of the avian foot (Aves).” *Zoology*, vol. 109, no. 5, pp. 281–293, 1990, doi: [10.1007/BF00312195](https://doi.org/10.1007/BF00312195).
- [7] L. Einoder and A. Richardson, “An ecomorphological study of the raptorial digital tendon locking mechanism,” *Ibis*, vol. 148, no. 3, pp. 515–525, 2006, doi: [10.1111/j.1474-919X.2006.00541.x](https://doi.org/10.1111/j.1474-919X.2006.00541.x).
- [8] L. Einoder and A. Richardson, “The digital tendon locking mechanism of owls: Variation in the structure and arrangement of the mechanism and functional implications,” *Emu*, vol. 107, no. 3, pp. 223–230, 2007, doi: [10.1071/MU06019](https://doi.org/10.1071/MU06019).
- [9] M. Kovac, “Learning from nature how to land aerial robots,” *Science*, vol. 352, no. 6288, pp. 895–896, 2016, doi: [10.1126/science.aaf6605](https://doi.org/10.1126/science.aaf6605).
- [10] C. E. Doyle et al., “An avian-inspired passive mechanism for quadrotor perching,” *IEEE/ASME Trans. Mechatron.*, vol. 18, no. 2, pp. 506–517, Apr. 2013, doi: [10.1109/TMECH.2012.2211081](https://doi.org/10.1109/TMECH.2012.2211081).
- [11] M. Burroughs, K. B. Freckleton, J. J. Abbott, and M. A. Minor, “A Sarrus-based passive mechanism for rotorcraft perching,” *J. Mechanisms Robot.*, vol. 8, no. 1, 2016, Art. no. 011010, doi: [10.1115/1.4030672](https://doi.org/10.1115/1.4030672).
- [12] P. M. Nadan et al., “A bird-inspired perching landing gear system,” *J. Mechanisms Robot.*, vol. 11, no. 6, 2019, Art. no. 061002, doi: [10.1115/1.4044416](https://doi.org/10.1115/1.4044416).
- [13] D. J. Dunlop and M. A. Minor, “Modeling and simulation of perching with a quadrotor aerial robot with passive bio-inspired legs and feet,” *Amer. Soc. Mech. Engineers Lett. Dyn. Syst. Control*, vol. 1, no. 2, 2021, Art. no. 021005, doi: [10.1115/1.4046778](https://doi.org/10.1115/1.4046778).
- [14] P. Xie, O. Ma, L. Zhang, and Z. Zhao, “A bio-inspired UAV leg-foot mechanism for landing, grasping and perching tasks,” in *Proc. Amer. Inst. Aeronaut. Astronaut. Atmospheric Flight Mechanics Conf.*, 2015, Art. no. 1689, doi: [10.2514/6.2015-1689](https://doi.org/10.2514/6.2015-1689).
- [15] W. R. T. Roderick, M. R. Cutkosky, and D. Lentink, “Bird-inspired dynamic grasping and perching in arboreal environments,” *Sci. Robot.*, vol. 6, no. 61, 2021, Art. no. eabj7562, doi: [10.1126/SCIROBOTICS.ABJ7562](https://doi.org/10.1126/SCIROBOTICS.ABJ7562).

- [16] H. Zhang, E. Lerner, B. Cheng, and J. Zhao, "Compliant bistable grippers enable passive perching for micro aerial vehicles," *IEEE/ASME Trans. Mechatron.*, vol. 26, no. 5, pp. 2316–2326, Oct. 2021, doi: [10.1109/TMECH.2020.3037303](https://doi.org/10.1109/TMECH.2020.3037303).
- [17] R. Zufferey, J. Tormo-Barbero, D. Feliu-Talegón, S. R. Nekoo, J. Á. Acosta, and A. Ollero, "How ornithopters can perch autonomously on a branch," *Nature Commun.*, vol. 13, no. 1, 2022, Art. no. 7713, doi: [10.1038/s41467-022-35356-5](https://doi.org/10.1038/s41467-022-35356-5).
- [18] H. Zhang, J. Sun, and J. Zhao, "Compliant bistable gripper for aerial perching and grasping," in *Proc. IEEE Int. Conf. Robot. Automat.*, 2019, pp. 1248–1253, doi: [10.1109/ICRA.2019.8793936](https://doi.org/10.1109/ICRA.2019.8793936).
- [19] T. G. Chen, K. A. W. Hoffmann, J. E. Low, K. Nagami, D. Lentink, and M. R. Cutkosky, "Aerial grasping and the velocity sufficiency region," *IEEE Robot. Automat. Lett.*, vol. 7, no. 4, pp. 10009–10016, Oct. 2022, doi: [10.1109/LRA.2022.3192652](https://doi.org/10.1109/LRA.2022.3192652).
- [20] A. X. Appius et al., "RAPTOR: Rapid aerial pickup and transport of objects by robots," in *Proc. IEEE Int. Conf. Intell. Robot. Syst.*, 2022, pp. 349–355, doi: [10.1109/IROS47612.2022.9981668](https://doi.org/10.1109/IROS47612.2022.9981668).
- [21] W. Stewart, L. Guarino, Y. Piskarev, and D. Floreano, "Passive perching with energy storage for winged aerial robots," *Adv. Intell. Syst.*, vol. 5, no. 4, 2021, Art. no. 2100150, doi: [10.1002/aisy.202100150](https://doi.org/10.1002/aisy.202100150).
- [22] H. T. Hsiao, J. Sun, H. Zhang, and J. Zhao, "A mechanically intelligent and passive gripper for aerial perching and grasping," *IEEE/ASME Trans. Mechatron.*, vol. 27, no. 6, pp. 5243–5253, Dec. 2022, doi: [10.1109/TMECH.2022.3175649](https://doi.org/10.1109/TMECH.2022.3175649).
- [23] A. Firouzeh, T. Higashisaka, K. Nagato, K. Cho, and J. Paik, "Stretchable Kirigami components for composite meso-scale robots," *IEEE Robot. Automat. Lett.*, vol. 5, no. 2, pp. 1883–1890, Apr. 2020, doi: [10.1109/LRA.2020.2969924](https://doi.org/10.1109/LRA.2020.2969924).
- [24] N. T. Jafferis, E. F. Helbling, M. Karpelson, and R. J. Wood, "Untethered flight of an insect-sized flapping-wing microscale aerial vehicle," *Nature*, vol. 570, pp. 491–495, 2019, doi: [10.1038/s41586-019-1322-0](https://doi.org/10.1038/s41586-019-1322-0).
- [25] S.-M. Baek, S. Yim, S.-H. Chae, D.-Y. Lee, and K.-J. Cho, "Ladybird beetle-inspired compliant origami," *Sci. Robot.*, vol. 5, no. 41, 2020, Art. no. eaaz6262, doi: [10.1126/scirobotics.aaz6262](https://doi.org/10.1126/scirobotics.aaz6262).
- [26] S. B. Diller, S. H. Collins, and C. Majidi, "The effects of electroadhesive clutch design parameters on performance characteristics," *J. Intell. Mater. Syst. Struct.*, vol. 29, no. 19, pp. 3804–3828, 2018, doi: [10.1177/1045389X18799474](https://doi.org/10.1177/1045389X18799474).
- [27] S. Diller, C. Majidi, and S. H. Collins, "A lightweight, low-power electroadhesive clutch and spring for exoskeleton actuation," in *Proc. IEEE Int. Conf. Robot. Automat.*, 2016, pp. 682–689, doi: [10.1109/ICRA.2016.7487194](https://doi.org/10.1109/ICRA.2016.7487194).
- [28] H. McClintonck, F. Z. Temel, N. Doshi, J. S. Koh, and R. J. Wood, "The milliDelta: A high-bandwidth, high-precision, millimeter-scale Delta robot," *Sci. Robot.*, vol. 3, no. 14, 2018, Art. no. eaar3018, doi: [10.1126/scirobotics.aar3018](https://doi.org/10.1126/scirobotics.aar3018).
- [29] S. Mintchev, M. Salerno, A. Cherpillod, S. Scaduto, and J. Paik, "A portable three-degrees-of-freedom force feedback origami robot for human–robot interactions," *Nature Mach. Intell.*, vol. 1, no. 12, pp. 584–593, 2019, doi: [10.1038/s42256-019-0125-1](https://doi.org/10.1038/s42256-019-0125-1).
- [30] J. Lee et al., "CaseCrawler: A lightweight and low-profile crawling phone case robot," *IEEE Robot. Automat. Lett.*, vol. 5, no. 4, pp. 5858–5865, Oct. 2020, doi: [10.1109/LRA.2020.3010205](https://doi.org/10.1109/LRA.2020.3010205).
- [31] C. Ha, Z. Zuo, F. B. Choi, and D. Lee, "Passivity-based adaptive backstepping control of quadrotor-type UAVs," *Robot. Auton. Syst.*, vol. 62, no. 9, pp. 1305–1315, 2014, doi: [10.1016/j.robot.2014.03.019](https://doi.org/10.1016/j.robot.2014.03.019).



Amir Firouzeh received the B.Sc. and M.Sc. degrees in mechanical engineering from Tehran and Sharif University, Tehran, Iran, in 2009 and 2012, respectively, and the Ph.D. degree in robotics, control, and intelligent systems from the Swiss Federal Institute of Technology, Lausanne, Switzerland, in 2017.

His research interests include soft robotics, novel sensing, actuation, and manufacturing technologies and their application in soft wearable devices.



Jongeun Lee received the B.S. degree in mechanical and aerospace engineering from Seoul National University, Seoul, South Korea, in 2016. He is currently working toward the Ph.D. degree in mechanical engineering with the Biorobotics Laboratory, Seoul National University, Seoul.

His current research interests include the design and fabrication of biologically inspired robots.



Hyunsoo Yang (Member, IEEE) received the B. S. and M. S. degrees in mechanical and aerospace engineering and the Ph.D. degree in mechanical engineering from Seoul National University, Seoul, South Korea, in 2012, 2014, and 2021, respectively.

He is currently a Postdoctoral Researcher with the Humanoids and Human Centered Mechatronics, Istituto Italiano di Tecnologia, Genova, Italy. His main research interests include dynamics and control of robotic systems with an emphasis on novel aerial robots, nonholonomic systems, and cooperative robots.



Dongjun Lee (Member, IEEE) received the B.S. degree in mechanical engineering and the M.S. degree in automation and design from the Korea Advanced Institute of Science and Technology, Daejeon, South Korea, in 1995 and 1997, respectively, and the Ph.D. degree in mechanical engineering from the University of Minnesota at Twin Cities, Minneapolis, MN, USA, in 2004.

He is currently a Professor with the Department of Mechanical Engineering, Seoul National University, Seoul, South Korea. His main research interests include the dynamics and control of robotic and mechatronic systems with emphasis on aerial/mobile robots, teleoperation/haptics, physics simulation, multirobot systems, and industrial control applications.



Kyu-Jin Cho (Member, IEEE) received the B.S and M.S. degrees in mechanical engineering from Seoul National University, Seoul, South Korea, in 1998 and 2000, respectively, and the Ph.D. degree in mechanical engineering from the Massachusetts Institute of Technology, Cambridge, MA, USA, in 2007.

He was a Postdoctoral Fellow with Harvard Microrobotics Laboratory until 2008. He is currently a Professor of mechanical engineering and the Director of BioRobotics Laboratory, Seoul National University, and the Director of Soft Robotic Research Center.

His research interests include biologically inspired robotics, soft robotics, soft wearable devices, novel mechanisms using smart structures, and rehabilitation/assistive robotics.

Dr. Cho was the recipient of the 2014 IEEE RAS Early Academic Career Award, 2014 ASME Compliant Mechanism Award, and 2013 IROS Best Video Award.